

Static analysis of laminated and sandwich composite doubly-curved shallow shells

Veysel Alankaya^{*1} and Ahmet Sinan Oktem^{2a}

¹ Department of Naval Architecture, Turkish Naval Academy, Tuzla 34942, Istanbul, Turkey

² Department of Mechanical Engineering, Gebze Technical University, Gebze 41400, Kocaeli, Turkey

(Received October 05, 2015, Revised December 07, 2015, Accepted January 04, 2016)

Abstract. A new analytical solution based on a third order shear deformation theory for the problem of static analysis of cross-ply doubly-curved shells is presented. The boundary-discontinuous generalized double Fourier series method is used to solve highly coupled linear partial differential equations with the mixed type simply supported boundary conditions prescribed on the edges. The complementary boundary constraints are introduced through boundary discontinuities generated by the selected boundary conditions for the derivation of the complementary solution. The numerical accuracy of the solution is compared by studying the comparisons of deflections, stresses and moments of symmetric and anti-symmetric laminated shells with finite element results using commercially available software under uniformly distributed load. Results are in good agreement with finite element counterparts. Additional results of the symmetric and anti-symmetric laminated and sandwich shells under single point load at the center and pressure load, are presented to provide data for the unsolved boundary conditions, benchmark comparisons and verifications.

Keywords: analytical solution; cross-ply shells; sandwich shells; boundary discontinuous Fourier analysis; higher order shear deformation theory; mixed simply supported

1. Introduction

The future prospective evolutions in the technology come up with the requirements of revolutionary materials. These requirements force to create advanced composites with their advantages relative to conventional materials such as high strength and stiffness to weight ratios, enhanced corrosion resistance and most importantly, the design flexibility inherent in composite laminates, known as tailoring, which is essentially exploiting the possibility of obtaining optimum design through a combination of structural /material concepts, stacking sequence, ply orientation, choice of the component phases, etc. to meet specific design requirements (Jones 1999 and Swanson 2001). The necessity of multifunctional materials in helicopters, planes, ships, multitasking vehicles etc. increased the research activities on composite materials. The stealth technology of ships for example, requires radar reflecting/absorbing mechanisms, acoustic absorbents or heat resistive insulators with highest electrical connectivity. Especially the recent

*Corresponding author, Ph.D., E-mail: valankaya@dho.edu.tr

^a Ph.D., E-mail: sinan.oktem@gyte.edu.tr

developments in marine and aerospace applications show that composite structures can be used to increase the operational performance to reduce the maintenance and fuel consumption costs (Loy and Lam 1999). Similar advantages also make composites attractive for a wide range of applications in marine, chemical, aerospace, automotive industries and for applications related to medical, energy and sporting goods (Swanson 2001).

Utilization of composite materials brings additional difficulties to the analyst such as the inter-laminar or transverse shear stress due to mismatch of material properties among layers, bending-stretching coupling due to asymmetry of lamination, and in-plane orthotropy and satisfying the specific boundary conditions in the solution. It has a valuable importance to know the effect of the design variable changes on the performance of composite laminates in various combinations of boundary conditions. It is also important to have appropriate techniques associated with good structural models to analyze the effects of design sensitivities efficiently and accurately (Youssif 2009).

The transverse stress and strain components are ignored in classical or thin shell theories which makes them highly inadequate for the analysis of even slightly thicker shells. The reliable prediction of deformations and stresses for the thicker structures requires the use of higher order shear deformation theories (Khalili *et al.* 2012 and Chen 2007). The groups of theories that are based on a cubic or higher expansion of the in-plane displacements introduce additional unknowns that are difficult to interpret in physical terms and require additional mathematical power for calculations.

Development of various new higher order deformation theories is an ongoing consistent effort. Cho *et al.* (1996) presented a refined theory assuming the combination of a zig-zag layer wise and cubic variation of in-plane displacement field. Applications of layer-wise theories for thick sandwich panels are presented by Demasi (2012, 2013). The requirements for the accurate description of stress and strain fields of different theories for the modeling of multilayered structures are given by Carrera (1999, 2000). Recent solutions to the problem of laminated composite beams, plates and shells using Carrera Unified Formulation (CUF) are presented comparing the results of different theories (Carrera *et al.* 2010, Catapano *et al.* 2011 and Ibrahim *et al.* 2012). Tornabene *et al.* (2014) presented the investigation on the static behavior of doubly curved laminated composite shells and panels based on CUF. Static analysis of doubly-curved laminated composite shells and panels under various loadings are presented by Viola *et al.* (2013a, b). The results of newly developed theories for composite shells / plates and functionally graded materials presented by Mantari *et al.* (2012a-d) and Zenkour (2013).

Very recently, the boundary conditions prescribed in this study published for laminated composite plates by Oktem *et al.* (2013). In the present work, plate solution (Oktem *et al.* 2013) is extended to cover the cross-ply doubly curved spherical and cylindrical panels. Displacement field by Reddy and Liu (1985) is used due to its simplicity and accuracy. The third-order assumption in the displacement field satisfies the zero shear stresses at the free surfaces, thus eliminating the need to compute shear correction factors, a requirement for the first order shear deformation theory (FSDT). The numerical accuracy of the present solution is also checked by studying its convergence characteristics, and also by comparison with the available FSDT-based finite element solution using commercially available software for symmetric and antisymmetric shells with two different material types under uniformly distributed load. Consequent results are presented for symmetric and antisymmetric laminated shells and by using two different material properties under uniformly distributed and a single point load at the center of the shell. The primary objective of the present study is to extend above-mentioned analysis for doubly curved spherical and

cylindrical panels and provide numerical results for a wide range of geometries. The novelty of this presentation is to develop prescribed solution methodology for hitherto unavailable arbitrary boundary conditions which cannot be solved by conventional Navier or Levy approaches. The boundary-discontinuous generalized double Fourier series method is used to solve highly coupled linear partial differential equations with the mixed type simply supported boundary conditions prescribed on the edges. The complementary boundary constraints are introduced through boundary discontinuities generated by the selected boundary conditions for the derivation of the complementary solution.

2. Statement of the problem

The laminated doubly curved shell, composed of finite number of orthotropic layers of uniform thickness of h is shown in Fig. 1. The ξ_1 and ξ_2 curves are lines of curvature on the shell mid-surface, $\xi_3 = \zeta = 0$, while $\xi_3 = \zeta$ is a straight line normal to the mid-surface. The displacement field by considering the cubic terms and satisfying the conditions of transverse shear stresses (and hence strains) vanishing at a point $(\xi_1, \xi_2, h/2)$ on the outer (top) and inner (bottom) surfaces of the shell, is given by Reddy and Liu (1985) as follows

$$u_1 = u(x_1, x_2, x_3) = u_0(x_1, x_2) + z\phi_1(x_1, x_2) - \frac{4}{3h^2}z^3\left(\phi_1 + \frac{\partial w_0}{\partial x_1}\right) \tag{1a}$$

$$u_2 = v(x_1, x_2, x_3) = v_0(x_1, x_2) + z\phi_2(x_1, x_2) - \frac{4}{3h^2}z^3\left(\phi_2 + \frac{\partial w_0}{\partial x_2}\right) \tag{1b}$$

$$u_3 = w(x_1, x_2, x_3) = w_0(x_1, x_2) \tag{1c}$$

where u, v, w represents displacements of a point at three axis (x_1, x_2, x_3) , while u_0, v_0, w_0 represents displacements of a point at the mid-surface ($z = 0$). The distance of the ply from the mid-surface and the thickness of the shell is represented by (z) and (h) respectively. ϕ_1 and ϕ_2 are rotations about x_2 and x_1 axes. The details of the strain-displacement relations, and other explanations were given in Reddy and Liu (1985).

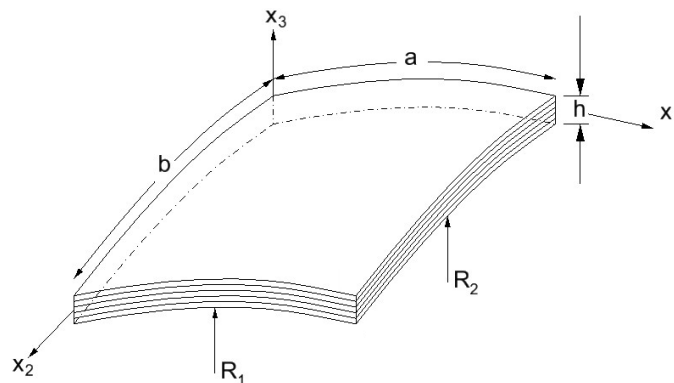


Fig. 1 Geometry of a laminated shell

The equilibrium equations derived using the principles of virtual work are given as follows

$$\frac{\partial N_1}{\partial x_1} + \frac{\partial N_6}{\partial x_2} = 0 \quad (2a)$$

$$\frac{\partial N_6}{\partial x_1} + \frac{\partial N_2}{\partial x_2} = 0 \quad (2b)$$

$$\frac{\partial Q_1}{\partial x_1} + \frac{\partial Q_2}{\partial x_2} - \frac{4}{h^2} \left(\frac{\partial K_1}{\partial x_1} + \frac{\partial K_2}{\partial x_2} \right) + \frac{4}{3h^2} \left(\frac{\partial^2 P_1}{\partial x_1^2} + \frac{\partial^2 P_2}{\partial x_2^2} + 2 \frac{\partial^2 P_6}{\partial x_1 \partial x_2} \right) - \frac{N_1}{R_1} - \frac{N_2}{R_2} = -p \quad (2c)$$

$$\frac{\partial M_1}{\partial x_1} + \frac{\partial M_6}{\partial x_2} - Q_1 + \frac{4}{h^2} K_1 - \frac{4}{3h^2} \left(\frac{\partial P_1}{\partial x_1} + \frac{\partial P_6}{\partial x_2} \right) = 0 \quad (2d)$$

$$\frac{\partial M_6}{\partial x_1} + \frac{\partial M_2}{\partial x_2} - Q_2 + \frac{4}{h^2} K_2 - \frac{4}{3h^2} \left(\frac{\partial P_6}{\partial x_1} + \frac{\partial P_2}{\partial x_2} \right) = 0 \quad (2e)$$

In Eq. (2c), p is the transverse load and N_i , M_i , P_i ($i = 1, 2, 6$) denotes stress resultants, stress couples and second stress couples (see, e.g., Reddy and Liu (1985)). Q_i , ($i = 1, 2$) represents the transverse shear stress resultants. They are given as follows

$$N_i = A_{ij} \varepsilon_j^0 + B_{ij} \kappa_j^0 + E_{ij} \kappa_j^2, \quad (i, j = 1, 2, 6) \quad (3a)$$

$$c N_i = A_{ij} \varepsilon_j^0 + B_{ij} \kappa_j^0 + E_{ij} \kappa_j^2, \quad (i, j = 1, 2, 6) \quad (3b)$$

$$P_i = E_{ij} \varepsilon_j^0 + F_{ij} \kappa_j^0 + H_{ij} \kappa_j^2 \quad (3c)$$

$$Q_1 = A_{5j} \varepsilon_j^0 + D_{5j} \kappa_j^1, \quad (j = 4, 5) \quad (4a)$$

$$Q_2 = A_{4j} \varepsilon_j^0 + D_{4j} \kappa_j^1 \quad (4b)$$

$$K_1 = D_{5j} \varepsilon_j^0 + F_{5j} \kappa_j^1 \quad (4c)$$

$$K_2 = D_{4j} \varepsilon_j^0 + F_{4j} \kappa_j^1 \quad (4d)$$

in which A_{ij} , B_{ij} , etc. are the laminate rigidities (integrated stiffnesses). These are given as follows

$$(A_{ij}, B_{ij}, D_{ij}) = \sum_{k=1}^N \int_{\xi_{k-1}}^{\xi_k} Q_{ij}^{(k)}(1, z, z^2) dz \quad (5a)$$

$$(E_{ij}, F_{ij}, H_{ij}) = \sum_{k=1}^N \int_{\xi_{k-1}}^{\xi_k} Q_{ij}^{(k)}(z^3, z^4, z^6) dz \tag{5b}$$

The distances to the mid-surface from plies through the thickness coordinate (z) are presented at Figs. 2(a) and (b) for laminated shells as the number of N plies and sandwich shells with core material.

Generalized stress – strain constitutive relations for an orthogonal lamina can be expressed as follows

$$\begin{Bmatrix} \sigma_1 \\ \sigma_2 \\ \sigma_6 \\ \sigma_5 \\ \sigma_4 \end{Bmatrix} = \begin{bmatrix} Q_{11} & Q_{12} & 0 & 0 & 0 \\ Q_{12} & Q_{22} & 0 & 0 & 0 \\ 0 & 0 & Q_{66} & 0 & 0 \\ 0 & 0 & 0 & Q_{55} & 0 \\ 0 & 0 & 0 & 0 & Q_{44} \end{bmatrix} \begin{Bmatrix} \varepsilon_1 \\ \varepsilon_2 \\ \varepsilon_6 \\ \varepsilon_5 \\ \varepsilon_4 \end{Bmatrix} \tag{6a}$$

in which $(\sigma_1, \sigma_2, \sigma_6, \sigma_5, \sigma_4)$ are the stress and $(\varepsilon_1, \varepsilon_2, \varepsilon_6, \varepsilon_5, \varepsilon_4)$ are the strain components (Reddy and Liu 1985) and the Q_{ij} expressions in terms of engineering constants are given below

$$Q_{11} = \frac{E_1}{1 - \nu_{12}\nu_{21}}, \tag{6b} \quad Q_{12} = \frac{\nu_{12}E_2}{1 - \nu_{12}\nu_{21}}, \tag{6c} \quad Q_{22} = \frac{E_2}{1 - \nu_{12}\nu_{21}}, \tag{6d}$$

$$Q_{66} = G_{12}, \tag{6e} \quad Q_{44} = G_{23}, \tag{6f} \quad Q_{55} = G_{13} \tag{6g}$$

Introduction of Eqs. (3a)-(3c) and (4a)-(4d) into Eqs. (2a)-(2e) gives five highly coupled fourth-order partial differential equations. The set of equations can be expressed in the following form

$$K_{ij}x_j = f_i \quad (i, j = 1, \dots, 5) \quad \text{and} \quad (K_{ij} = K_{ji}) \tag{7a}$$

where

$$\{x_j\}^T = \{u_1 \quad u_2 \quad u_3 \quad \phi_1 \quad \phi_2\} \tag{7b}$$

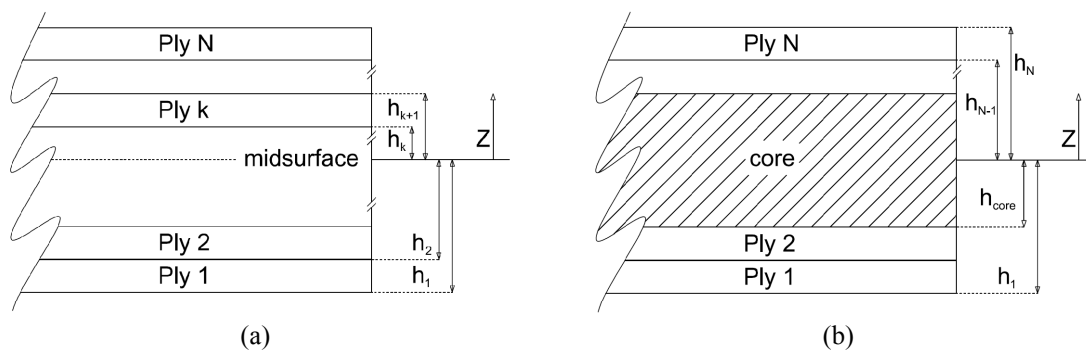


Fig. 2 The distances to the mid-surface from plies for (a) Laminated; and (b) sandwich shell

$$\{f_i\}^T = \{0 \quad 0 \quad -Q_{mn} \quad 0 \quad 0\} \quad (7c)$$

and $[K_{ij}]$ are given in Appendix A.

The problem under consideration is solved for the following boundary conditions:

The simply supported type 1 (SS1) boundary conditions are prescribed at the edges $x_1 = 0, a$

$$N_1 = N_6 = u_3 = M_1 = P_1 = \phi_2 = 0 \quad (8a)$$

and, the simply supported type 4 (SS4) boundary conditions prescribed at the edges $x_2 = 0, b$

$$u_1 = u_2 = u_3 = \phi_1 = M_2 = P_2 = 0 \quad (8b)$$

3. Solution procedure

The particular solution to the boundary value problem of the partial differential equations given by Eq. (7a), in conjunction with the admissible boundary conditions given by Eqs. (8a)-(8b) is assumed as follows

$$u_1(x_1, x_2) = \sum_{m=0}^{\infty} \sum_{n=1}^{\infty} U_{mn} f_1(x_1, x_2) \quad 0 \leq x_1 \leq a; \quad 0 \leq x_2 \leq b \quad (9a)$$

$$u_2(x_1, x_2) = \sum_{m=1}^{\infty} \sum_{n=0}^{\infty} V_{mn} f_2(x_1, x_2), \quad 0 < x_1 < a; \quad 0 < x_2 < b \quad (9b)$$

$$u_3(x_1, x_2) = \sum_{m=1}^{\infty} \sum_{n=1}^{\infty} W_{mn} f_3(x_1, x_2), \quad 0 \leq x_1 \leq a; \quad 0 \leq x_2 \leq b \quad (9c)$$

$$\phi_1(x_1, x_2) = \sum_{m=0}^{\infty} \sum_{n=1}^{\infty} X_{mn} f_1(x_1, x_2), \quad 0 \leq x_1 \leq a; \quad 0 \leq x_2 \leq b \quad (9d)$$

$$\phi_2(x_1, x_2) = \sum_{m=1}^{\infty} \sum_{n=0}^{\infty} Y_{mn} f_2(x_1, x_2), \quad 0 \leq x_1 \leq a; \quad 0 \leq x_2 \leq b \quad (9e)$$

where

$$f_1(x_1, x_2) = \cos(\alpha x_1) \sin(\beta x_2), \quad (10a)$$

$$f_2(x_1, x_2) = \sin(\alpha x_1) \cos(\beta x_2), \quad (10b)$$

$$f_3(x_1, x_2) = \sin(\alpha x_1) \sin(\beta x_2), \quad (10c)$$

$$\alpha = \frac{m\pi}{a}, \quad \beta = \frac{n\pi}{b}. \quad (10d)$$

Numerical results are provided for the uniformly distributed load and the point load at the center of the panel and the load term given in Eq. (7c) is defined as follows

$$Q_{mn} = \frac{16p}{\pi^2 mn} \quad (\text{Uniformly distributed load}) \tag{11a}$$

$$Q_{mn} = \frac{4p}{ab} \sin\left(\frac{m\pi}{2}\right) \sin\left(\frac{n\pi}{2}\right) \quad (\text{Point load at the center}) \tag{11b}$$

Introduction of assumed displacement functions into the partial differential equations given by Eq. (7a) generates $5mn + 2m + 2n$ unknown (panel or interior) Fourier coefficients. The next step is comprised of partial differentiation of the assumed particular solution functions. The procedure for differentiation of these functions is based on Lebesgue integration theory that introduces boundary Fourier coefficients arising from discontinuities. The function u_2 given by Eq. (9b) vanishes at the edges, at $x_1 = 0, a$, thus violating the complementary boundary constraint at these edges. Therefore, for further differentiation, $u_{2,1}$ is first expanded in double Fourier series, in the form suggested by Chaudhuri (2002) in order to satisfy the complementary boundary constraint (inequality). The partial derivatives which cannot be obtained by term wise differentiation are obtained as follows

$$u_{2,1} = \frac{1}{4} \bar{a}_0 + \frac{1}{2} \sum_{n=1}^{\infty} \bar{a}_n \cos(\beta x_2) + \frac{1}{2} \sum_{m=1}^{\infty} [\alpha V_{m0} + \gamma_m \bar{a}_0 + \psi_m \bar{b}_0] \cos(\alpha x_1) + \sum_{m=1}^{\infty} \sum_{n=1}^{\infty} [\alpha V_{mn} + \gamma_m \bar{a}_n + \psi_m \bar{b}_n] \cos(\alpha x_1) \cos(\beta x_2) \tag{12}$$

In a similar manner u_2 is forced to vanish at the edges, $x_2 = 0$ and b . The derivatives of u_2 are given in Eqs. (13a) and (13b).

$$u_{2,2} = - \sum_{m=1}^{\infty} \sum_{n=1}^{\infty} \beta V_{mn} \sin(\alpha x_1) \sin(\beta x_2) \tag{13a}$$

$$u_{2,22} = \frac{1}{2} \sum_{m=1}^{\infty} \bar{c}_m \sin(\alpha x_1) + \sum_{m=1}^{\infty} \sum_{n=1}^{\infty} [-\beta^2 V_{mn} + \gamma_n \bar{c}_m + \psi_n \bar{d}_m] \sin(\alpha x_1) \cos(\beta x_2) \tag{13b}$$

in which

$$(\gamma_n, \psi_n) = \begin{cases} (0,1), & n = \text{odd}, \\ (1,0), & n = \text{even}. \end{cases} \tag{14}$$

The unknown boundary Fourier coefficients, \bar{a}_n, \bar{c}_m etc., appear in Eqs. (12) and (13), are defined as follows

$$\bar{a}_n, \bar{b}_n = \frac{4}{ab} \int_0^b [u_2(a, x_2) \mp u_2(0, x_2)] \cos(\beta x_2) dx_2 \tag{15a}$$

$$\bar{c}_m, \bar{d}_m = \frac{4}{ab} \int_0^a [u_{2,2}(x_1, b) \mp u_{2,2}(x_1, 0)] \sin(\alpha x_1) dx_1 \tag{15b}$$

The remaining partial derivatives can be obtained by term-wise differentiation. The above step generates additional $2m + 2n + 2$ unknown (boundary) Fourier coefficients. The remaining equations are supplied by the geometric and natural boundary conditions. The geometric boundary conditions relating to u_3 , ϕ_2 and the natural boundary conditions relating to N_1 , M_1 and P_1 are satisfied a priori at the edges $x_1 = 0, a$. In order to match the number of unknown constant coefficients, remaining equations are obtained from satisfying the natural boundary conditions relating to N_6 , as shown below

$$\sum_{n=1}^{\infty} \cos(\beta x_2) \left\{ \begin{aligned} & \frac{A_{66}}{2} \beta U_{0n} + a_1 \beta X_{0n} + \frac{A_{66}}{2} \bar{a}_n \\ & + \sum_{m=1}^{\infty} A_{66} (\alpha V_{mn} + \gamma_m \bar{a}_n + \psi_m \bar{b}_n) \bar{H} + \sum_{m=1}^{\infty} A_{66} \beta U_{mn} \bar{H} \\ & + \sum_{m=1}^{\infty} \beta X_{mn} a_1 \bar{H} + \sum_{m=1}^{\infty} \alpha Y_{mn} a_1 \bar{H} - \sum_{m=1}^{\infty} \alpha \beta W_{mn} a_2 \bar{H} / 2 \end{aligned} \right\} = 0 \tag{16a}$$

$$\sum_{m=1}^{\infty} \left\{ \frac{A_{66}}{2} [\alpha V_{m0} + \gamma_m \bar{a}_0 + \psi_m \bar{b}_0] \bar{H} + \alpha Y_{m0} a_1 \bar{H} \right\} + A_{66} \bar{a}_0 / 4 = 0 \tag{16b}$$

in which for the case of N_6 at the boundaries $x_1 = 0$ and a , $\bar{H} = 1$ and $\bar{H} = (-1)^m$, respectively.

For the computational purpose, Eqs. (16a)-(16b) can be rewritten in more useful forms as follows:

For all values of $n = 1, 2, \dots$

$$\sum_{m=1,3,5,\dots}^{\infty} \left\{ \frac{A_{66}}{2} [\alpha V_{m0} + \bar{b}_0] + \alpha Y_{m0} a_1 \right\} \psi_m = 0 \tag{17a}$$

$$\sum_{m=2,4,6,\dots}^{\infty} \left\{ \frac{A_{66}}{2} [\alpha V_{m0} + \bar{a}_0] + \alpha Y_{m0} a_1 \right\} \gamma_m + A_{66} \bar{a}_0 / 4 = 0 \tag{17b}$$

$$\sum_{m=1,3,5,\dots}^{\infty} \left\{ A_{66} [\alpha V_{mn} + \bar{b}_n] + A_{66} \beta U_{mn} + \alpha Y_{mn} a_1 + \beta X_{mn} a_1 - a_2 \alpha \beta W_{mn} / 2 \right\} \psi_m = 0 \tag{17c}$$

$$\begin{aligned} \sum_{m=2,4,6,\dots}^{\infty} \left\{ A_{66} [\alpha V_{mn} + \bar{a}_n] + A_{66} \beta U_{mn} + \alpha Y_{mn} a_1 + \beta X_{mn} a_1 - \frac{a_2}{2} \alpha \beta W_{mn} \right\} \gamma_m \\ + \frac{A_{66}}{2} (\bar{a}_n + 2\beta U_{0n}) + \beta X_{0n} a_1 = 0. \end{aligned} \tag{17d}$$

where a_1 and a_2 are constants in Eqs. (16)-(17) and they are given as follows

$$a_1 = B_{66} - c_1 E_{66}, \quad (18e) \quad a_2 = 2c_1 E_{66} \quad (18f) \quad \text{and} \quad c_1 = 4/3h^2 \quad (18g)$$

Additionally, the geometric boundary conditions relating to u_1, u_3, ϕ_1 and the natural boundary conditions relating to M_2 and P_2 are also satisfied a priori at the edges $x_2 = 0, b$. Satisfying the geometric boundary conditions given by Eq. (8b) such that u_2 should vanish at the edges $x_2 = 0, b$ and equating the coefficients of $\sin(\alpha x)$ yield the following algebraic equations:

For all values of $m = 1, 2, \dots$

$$\sum_{n=1,3,5,\dots}^{\infty} \psi_n V_{mn} = 0 \quad (19a) \quad \text{and} \quad V_{m0} + \sum_{n=2,4,6,\dots}^{\infty} \gamma_n V_{mn} = 0 \quad (19b)$$

Finally, the above operations result in, in total, $5mn + 4m + 4n + 2$ linear algebraic equations in as many unknowns and furnish a complete solution to the boundary value problem considered here.

4. Numerical results and discussions

Numerical results are presented for symmetric ($[0^\circ/90^\circ/0^\circ]$) and anti-symmetric $[0^\circ/90^\circ]$ cross-ply doubly-curved of rectangular spherical shells ($a = b$), which are subjected to uniformly distributed and single point loads. The following material properties are assumed

- (a) Material type I : $E_1 = 105.47 \text{ GPa (15.000 ksi)}, \quad E_1/E_2 = 15, \quad \nu_{12} = 0.40,$
 $G_{12}/E_2 = G_{13}/E_2 = 0.42865, \quad G_{23}/E_2 = 0.3429$
- (b) Material type II : $E_1 = 132.384 \text{ GPa (19.200 ksi)}, \quad E_1/E_2 = 12.31, \quad \nu_{12} = 0.24,$
 $G_{12}/E_2 = G_{13}/E_2 = 0.526, \quad G_{23}/E_2 = 0.335$

Thickness ratio of the core material (C/h) is chosen as the deterministic variable for the analyses of sandwich shells and the following material properties are assumed for core material

$$\begin{aligned} \text{Core material} \quad E_1 &= 35 \text{ GPa (5.000 ksi)}, & E_1/E_2 &= 5, & \nu_{12} &= 0.25, \\ G_{12}/E_2 &= G_{13}/E_2 = 2, & G_{23}/E_2 &= 0.2 \end{aligned}$$

Here E_1 and E_2 are the in-plane Young's moduli in x_1 and x_2 coordinate directions, respectively, while G_{12} denotes in-plane shear modulus. G_{13} and G_{23} are transverse shear moduli in the x_1 - x_3 and x_2 - x_3 planes, respectively, while ν_{12} is major Poisson's ratio on the x_1 - x_2 plane. In the calculations, the following normalized quantities are defined

$$u_1^* = (10^3 E_2 h^3 / p_0 a^4) u_1, \quad (20a) \quad u_2^* = (10^3 E_2 h^3 / p_0 a^4) u_2, \quad (20b)$$

$$u_3^* = (10^3 E_2 h^3 / p_0 a^4) u_3, \quad (20c) \quad \phi_1^* = (10^2 E_2 h^3 / p_0 a^3) \phi_1, \quad (20d)$$

$$\phi_2^* = (10^2 E_2 h^3 / p_0 a^3) \phi_2, \quad (20e) \quad M_1^* = (10^3 / p_0 a^2) M_1, \quad (20f)$$

$$M_2^* = (10^3 / p_0 a^2) M_2, \quad (20c) \quad \sigma_1^* = 10(h^2 / p_0 b^2) \sigma_1, \quad (20d)$$

$$\sigma_2^* = 10(h^2 / p_0 b^2) \sigma_2, \quad (20c) \quad \sigma_6^* = 10(h / p_0 a) \sigma_6 \quad (20d)$$

in which 'a' is one side of the panel, and p_0 denotes the transverse load. For all the numerical results presented in all tables and figures except the Fig. 9, the normalized quantities are computed at the center of the panel.

Fig. 3 displays the convergence of normalized central transverse displacement u_3^* and moment M_1^* of a moderately thick ($a/h = 10$) anti-symmetric cross-ply $[0^\circ/90^\circ]$ plate, computed using the present HSDT with the material type I under uniformly distributed load. The normalized displacement (u_3^*) and moment (M_1^*) exhibit a fast convergence at approximately $m = n = 10$. Therefore the value for $m = n = 10$ is used for the results obtained from presented methodology in the numerical applications.

4.1. Layered composite material

The normalized central deflections, u_3^* and the central moments, M_1^* and M_2^* obtained using the present solution for the anti-symmetric $[0^\circ/90^\circ]$ and symmetric $[0^\circ/90^\circ/0^\circ]$ spherical shells

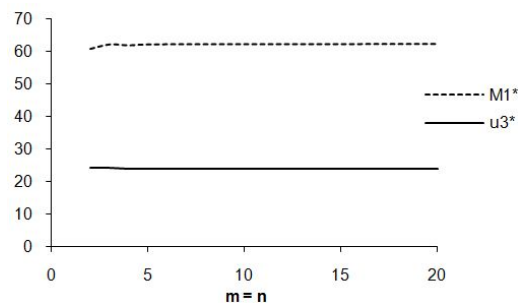


Fig. 3 Convergence of normalized central deflection, u_3^* and moment M_1^* , of an antisymmetric moderately thick cross-ply $[0^\circ/90^\circ]$ shell

Table 1 Central deflections of cross-ply symmetric shells under concentrated point load at the center

| Thickness | Ref. ⁽¹⁾ | Ref. ⁽²⁾ | Present |
|-----------|---------------------|---------------------|---------|
| 0.32 | 3.9274 | 3.8812 | 8.4529 |
| 1.6 | 0.1722 | 0.1723 | 0.2569 |
| 3.2 | 0.0371 | 0.0379 | 0.0414 |
| 6.4 | 0.0091 | 0.0080 | 0.0075 |

⁽¹⁾ Reddy and Liu 1985

⁽²⁾ Tornabene et.al. 2015

Note: The material and geometrical properties are taken from referenced studies and applied to present theory

with different a/h and R/L ratios for the material types I and II under uniformly distributed and single point loads at the center are presented in Tables 2-3, respectively. Plate results, which are published earlier in (Oktem *et al.* 2013), are regenerated using the new material properties provided in this paper for comparison purposes. A finite element model of the shell is also prepared by utilizing the available finite element software ANSYS. The finite element shell model and the layers of the shell for a symmetric $[0^\circ/90^\circ/90^\circ/0^\circ]$ lay-up are given in Figs. 4 and 5, respectively.

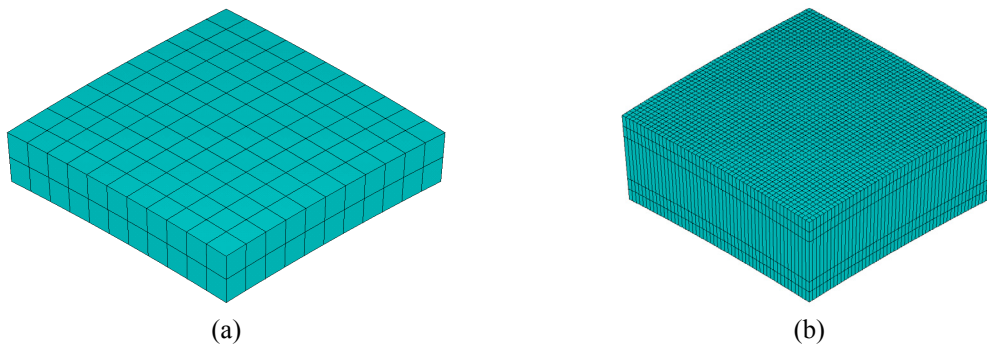


Fig. 4 Finite element model of the shell

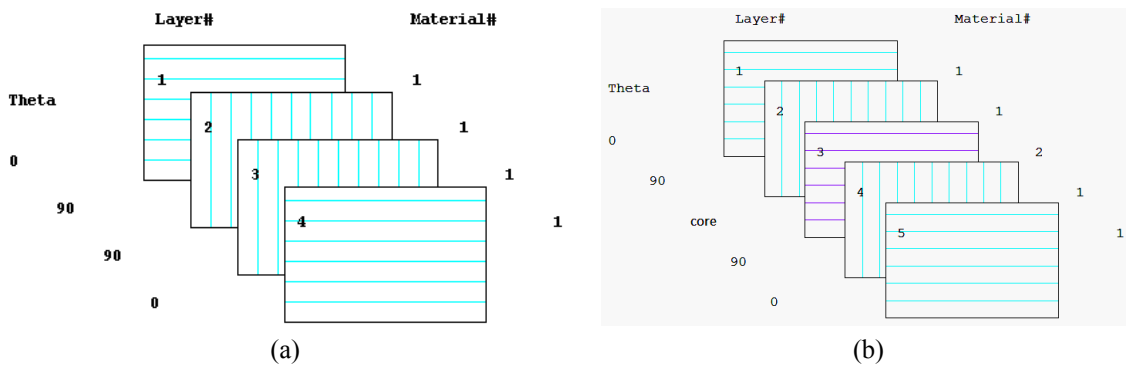


Fig. 5 Schematic of layers of a symmetric $[0^\circ/90^\circ/90^\circ/0^\circ]$ shell model

Table 2 Normalized central deflections and moments of cross-ply anti-symmetric $[0^\circ/90^\circ]$ shells under uniformly distributed and single point load for material type I and type II

| Load | Material | R/L | a/h | | | | | | |
|----------------------------|------------|--------------------|-------|-------|-------|-------|-------|-------|-------|
| | | | 5 | 10 | 20 | 30 | 40 | 50 | |
| Uniformly distributed load | Material I | u_3^* | 10 | 30.28 | 23.92 | 21.69 | 20.29 | 18.77 | 17.15 |
| | | | 50 | 30.32 | 24.10 | 22.53 | 22.22 | 22.07 | 21.95 |
| | | Plate ¹ | 10 | 30.30 | 24.08 | 22.52 | 22.23 | 22.13 | 22.08 |
| | | | 50 | 61.74 | 62.17 | 61.55 | 59.21 | 55.59 | 51.17 |
| | | M_1^* | 10 | 61.34 | 62.57 | 61.93 | 62.18 | 62.34 | 62.42 |
| | | | 50 | 61.18 | 61.22 | 61.27 | 61.28 | 61.29 | 61.29 |

Table 2 Normalized central deflections and moments of cross-ply anti-symmetric $[0^\circ/90^\circ]$ shells under uniformly distributed and single point load for material type I and type II

| Load | Material | R/L | a/h | | | | | | |
|---------------------------------|--------------------|--------------------|--------------------|-------|-------|-------|-------|-------|-------|
| | | | 5 | 10 | 20 | 30 | 40 | 50 | |
| Uniformly distributed load | Material I | M_2^* | 10 | 59.19 | 56.99 | 51.58 | 45.31 | 38.75 | 32.37 |
| | | | 50 | 60.76 | 60.46 | 59.76 | 58.95 | 58.06 | 57.12 |
| | | | Plate ¹ | 61.10 | 61.16 | 61.23 | 61.25 | 61.26 | 61.26 |
| | u_3^* | 10 | 79.82 | 65.95 | 62.54 | 61.91 | 61.65 | 61.45 | |
| | | 50 | 79.73 | 65.84 | 62.39 | 61.77 | 61.57 | 61.49 | |
| | | Plate ¹ | 79.71 | 65.80 | 62.32 | 61.68 | 61.45 | 61.35 | |
| | Material II | M_1^* | 10 | 71.57 | 71.83 | 71.71 | 71.35 | 70.82 | 70.16 |
| | | | 50 | 71.60 | 71.90 | 72.00 | 72.01 | 72.00 | 71.98 |
| | | | Plate ¹ | 71.60 | 71.91 | 72.02 | 72.04 | 72.05 | 72.05 |
| | | M_2^* | 10 | 71.52 | 71.74 | 71.60 | 71.28 | 70.87 | 70.38 |
| | | | 50 | 71.58 | 71.87 | 71.96 | 71.95 | 71.92 | 71.88 |
| | | | Plate ¹ | 71.59 | 71.90 | 72.01 | 72.03 | 72.04 | 72.04 |
| Single point load at the center | u_3^* | 10 | 11.37 | 7.66 | 6.34 | 5.80 | 5.35 | 4.89 | |
| | | 50 | 11.38 | 7.71 | 6.56 | 6.30 | 6.20 | 6.13 | |
| | | Plate ¹ | 11.38 | 7.71 | 6.56 | 6.31 | 6.21 | 6.17 | |
| | Material I | M_1^* | 10 | 0.60 | 0.59 | 0.57 | 0.56 | 0.54 | 0.53 |
| | | | 50 | 0.60 | 0.58 | 0.56 | 0.56 | 0.55 | 0.55 |
| | | | Plate ¹ | 0.60 | 0.58 | 0.56 | 0.55 | 0.55 | 0.55 |
| | | M_2^* | 10 | 0.59 | 0.56 | 0.53 | 0.51 | 0.48 | 0.46 |
| | | | 50 | 0.60 | 0.58 | 0.56 | 0.55 | 0.54 | 0.53 |
| | | | Plate ¹ | 0.60 | 0.58 | 0.56 | 0.55 | 0.55 | 0.55 |
| | Material II | u_3^* | 10 | 30.53 | 20.96 | 18.05 | 17.42 | 17.15 | 16.98 |
| | | | 50 | 30.51 | 20.94 | 18.03 | 17.43 | 17.21 | 17.10 |
| | | | Plate ¹ | 30.51 | 20.93 | 18.02 | 17.40 | 17.18 | 17.07 |
| M_1^* | | 10 | 0.63 | 0.63 | 0.63 | 0.62 | 0.62 | 0.61 | |
| | | 50 | 0.63 | 0.63 | 0.63 | 0.63 | 0.62 | 0.62 | |
| | | Plate ¹ | 0.63 | 0.63 | 0.63 | 0.63 | 0.62 | 0.62 | |
| M_2^* | 10 | 0.63 | 0.63 | 0.63 | 0.62 | 0.62 | 0.61 | | |
| | 50 | 0.63 | 0.63 | 0.63 | 0.62 | 0.62 | 0.62 | | |
| | Plate ¹ | 0.63 | 0.63 | 0.63 | 0.63 | 0.62 | 0.62 | | |

Plate¹ : Plate results are regenerated for comparison purposes

The difference between the present solution and the finite element results are close for both anti-symmetric and symmetric laminations and for both material types. The comparisons of the present results with finite element counterparts for normalized stresses (σ_1^* , σ_2^*) and normalized deflections (u_3^*) with a/h ratio are presented in Figs. 6, 7 and 8, respectively, for the material type I. There are small differences for both stress and deflection results between the present and the finite element counterparts.

Table 3 Normalized central deflections and moments of cross-ply symmetric [0°/90°/0°] shells under uniformly distributed and single point load for material type I and type II

| Load | Material | R/L | a/h | | | | | | |
|---------------------------------|-------------|---------|--------------------|--------|--------|--------|--------|--------|--------|
| | | | 5 | 10 | 20 | 30 | 40 | 50 | |
| Uniformly Distributed Load | Material I | u_3^* | 10 | 23.08 | 13.61 | 10.89 | 10.15 | 9.64 | 9.16 |
| | | | 50 | 23.15 | 13.70 | 11.13 | 10.63 | 10.45 | 10.45 |
| | | | Plate ¹ | 23.15 | 13.71 | 11.71 | 10.65 | 10.48 | 10.48 |
| | | M_1^* | 10 | 107.74 | 117.33 | 118.43 | 115.68 | 111.46 | 106.29 |
| | | | 50 | 108.08 | 118.21 | 121.34 | 121.82 | 121.84 | 121.68 |
| | | | Plate ¹ | 108.10 | 118.25 | 121.47 | 122.09 | 122.31 | 122.31 |
| | | M_2^* | 10 | 23.14 | 16.08 | 13.52 | 12.68 | 12.02 | 11.37 |
| | | | 50 | 23.22 | 16.21 | 13.86 | 13.38 | 13.19 | 13.08 |
| | | | Plate ¹ | 23.22 | 16.21 | 13.88 | 13.41 | 13.24 | 13.16 |
| | Material II | u_3^* | 10 | 77.56 | 63.60 | 60.06 | 59.33 | 59.00 | 58.75 |
| | | | 50 | 77.57 | 63.62 | 60.13 | 59.48 | 59.25 | 59.14 |
| | | | Plate ¹ | 77.57 | 63.62 | 60.13 | 59.49 | 59.26 | 59.16 |
| | | M_1^* | 10 | 83.90 | 84.64 | 84.71 | 84.45 | 84.03 | 83.49 |
| | | | 50 | 83.92 | 84.70 | 84.96 | 85.00 | 85.01 | 84.99 |
| | | | Plate ¹ | 83.92 | 84.71 | 84.97 | 85.03 | 85.05 | 85.06 |
| | | M_2^* | 10 | 59.38 | 59.23 | 59.13 | 59.01 | 58.85 | 58.66 |
| | | | 50 | 59.38 | 59.25 | 59.22 | 59.21 | 59.20 | 59.19 |
| | | | Plate ¹ | 59.38 | 59.26 | 59.22 | 59.22 | 59.21 | 59.21 |
| Single Point Load at the Center | Material I | u_3^* | 10 | 10.24 | 5.34 | 3.74 | 3.33 | 3.11 | 2.94 |
| | | | 50 | 10.26 | 5.37 | 3.80 | 3.46 | 3.33 | 3.26 |
| | | | Plate ¹ | 10.26 | 5.37 | 3.81 | 3.47 | 3.34 | 3.28 |
| | | M_1^* | 10 | 0.81 | 0.84 | 0.87 | 0.88 | 0.88 | 0.87 |
| | | | 50 | 0.81 | 0.85 | 0.88 | 0.89 | 0.90 | 0.91 |
| | | | Plate ¹ | 0.81 | 0.85 | 0.88 | 0.89 | 0.91 | 0.92 |
| | | M_2^* | 10 | 0.32 | 0.31 | 0.31 | 0.31 | 0.30 | 0.30 |
| | | | 50 | 0.32 | 0.31 | 0.31 | 0.31 | 0.31 | 0.30 |
| | | | Plate ¹ | 0.32 | 0.31 | 0.31 | 0.31 | 0.31 | 0.30 |
| | Material II | u_3^* | 10 | 30.08 | 20.41 | 17.44 | 16.78 | 16.50 | 16.32 |
| | | | 50 | 30.08 | 20.42 | 17.47 | 16.85 | 16.62 | 16.51 |
| | | | Plate ¹ | 30.08 | 20.42 | 17.48 | 16.86 | 16.63 | 16.52 |
| | | M_1^* | 10 | 0.71 | 0.71 | 0.71 | 0.71 | 0.70 | 0.70 |
| | | | 50 | 0.72 | 0.72 | 0.71 | 0.71 | 0.70 | 0.70 |
| | | | Plate ¹ | 0.72 | 0.72 | 0.71 | 0.71 | 0.70 | 0.70 |
| | | M_2^* | 10 | 0.56 | 0.55 | 0.55 | 0.55 | 0.55 | 0.54 |
| | | | 50 | 0.56 | 0.55 | 0.55 | 0.55 | 0.55 | 0.55 |
| | | | Plate ¹ | 0.56 | 0.55 | 0.55 | 0.55 | 0.55 | 0.55 |

Plate¹ : Plate results are regenerated for comparison purposes

Nevertheless, the difference in Figs. 6 and 7 between presented theory and FEA results are higher at moderately thick regime because of the methodology used in FEA software which is based on FSDT. Therefore the difference in moderately thick regime is the result of the accuracy of these theories. Contrary to expectations, normalized central deflection (u_3^*) at thin shell regime diverges from FEA solution for $R/L = 10$ in decreasing thickness. This anomaly can be explained as the effect of element description in FEA software. Due to the presented theory is mainly focused on the effects of shear deformations which are more efficient in the thick and moderately thick regime, Shell-91 element is used which is developed for modeling thick sandwich structures and layered applications of structural shells. Laminate properties are defined by specifying individual layer properties. Since the average layer properties are used, shell element only relates generalized forces and moments to obtain strains and curvatures on meso-scale level. Shell-91 element type with 8 nodes and six degree of freedom is suitable for nonlinear layered structural shell analyses

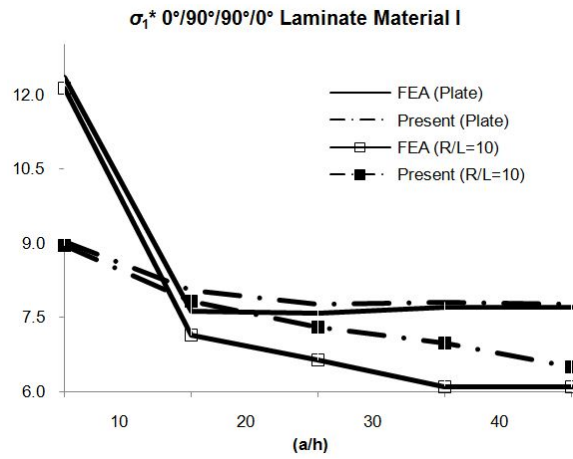


Fig. 6 Comparison of normalized stress σ_1^* with finite element solution for material type I, under uniformly distributed load for symmetric $[0^\circ/90^\circ/90^\circ/0^\circ]$ laminate

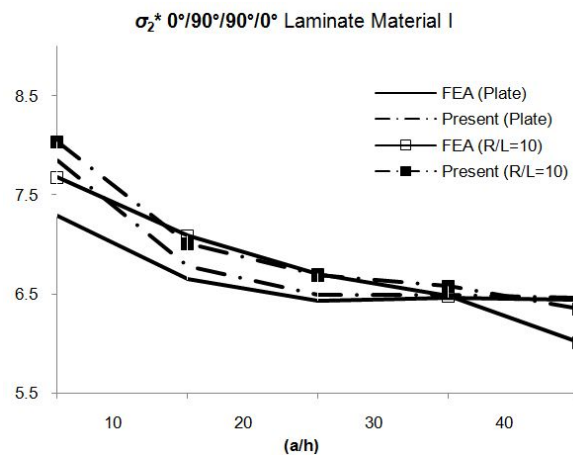


Fig. 7 Comparison of normalized stress σ_2^* with finite element solution for material type I, under uniformly distributed load for symmetric $[0^\circ/90^\circ/90^\circ/0^\circ]$ laminate

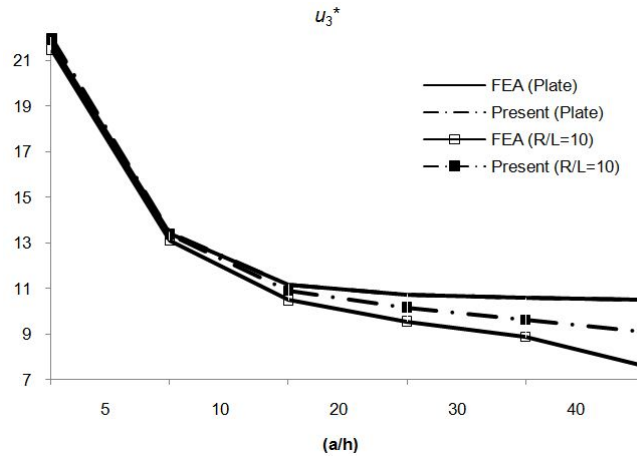


Fig. 8 Comparison of normalized deflection (u_3^*) with finite element solution for material type I, under uniformly distributed load for symmetric $[0^\circ/90^\circ/90^\circ/0^\circ]$ laminate

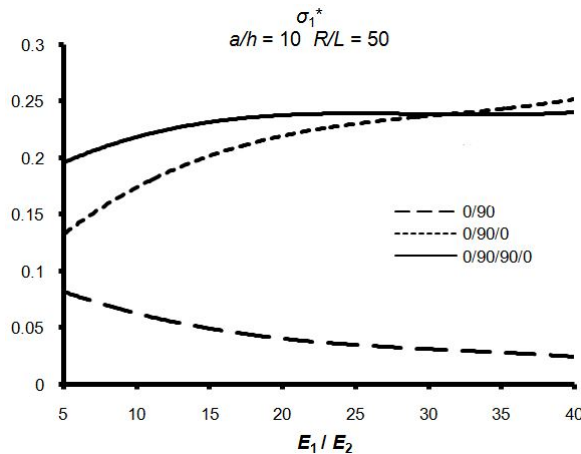


Fig. 9 Variation of normalized stress σ_1^* with E_1/E_2 ratio for symmetric and antisymmetric laminate under point load at the center for material type I, $a/h = 10$ and $R/L = 50$

with its sandwich option. Because the chosen element type is considered for comparison purposes on meso-scale level, each ply is modeled and analyzed having one element per ply. However modeling of each ply by more than three elements causes more accurate results of nodal displacements included in the overall nodal solution.

Concentrated central loads are not analyzed by FEA software because Tornabene *et al.* (2015) recently presented that the problem of concentrated loads does not give uniquely results as far as thick shells are considered. Moreover, effect of concentrated load at the center of the panel is investigated by the comparison of literature results at Table 1. (Note that, for the analyses presented at Table 1, the material and the geometrical properties are taken from referenced studies therefore it differs from presented results in this study). However the differences between the results of Reddy and Liu 1985, Tornabene *et al.* 2015 and present theory are mostly caused by the

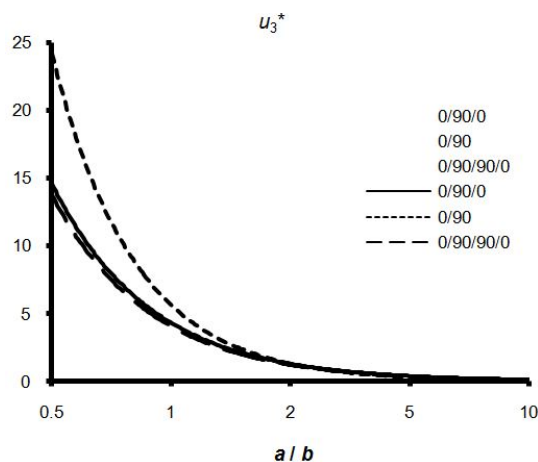


Fig. 10 Variation of normalized deflection (u_3^*) with a/b ratio for symmetric and antisymmetric laminates under point load at the center for material type I, $a/h = 10$ and $R/L = 50$

effects of boundary conditions.

Fig. 9 shows the variation of in-plane normalized stress, σ_1^* with E_1/E_2 ratio for symmetric and anti-symmetric laminations and for material type I for a moderately thick shallow shell. The difference between the symmetric and anti-symmetric laminates is clearly visible in this plot and the difference is progressively increasing with higher values of E_1/E_2 ratio.

Variation of normalized central deflection with a/b ratio for symmetric and anti-symmetric laminations is presented in Fig. 10 under point load at the center for a moderately thick ($a/h = 10$) shallow shell. The difference between symmetric and anti-symmetric laminates are negligible for ratio $a/b > 2$. But this difference becomes prominent for smaller values of a/b ratio, which is a clear and dominant effect of the two different boundary conditions on the opposite edges of the panel.

Variations of the normalized response quantities of interest such as u_1^* , u_3^* , M_1^* and ϕ_1^* , of moderately thick ($a/h = 10$) symmetric $[0^\circ/90^\circ/0^\circ]$ spherical shell, computed at and along $x_2 = 0$ to b are shown in Fig. 11. The normalized deflection, u_3^* and central moment, M_1^* assumes their respective maximum magnitude at the center of the shell, where the surface-parallel displacement, u_1^* and rotation, ϕ_1^* vanishes. It is also important to note that this plot clearly indicates the satisfaction of the boundary conditions dictated by the boundary discontinuous double Fourier series approach used in the present analysis.

The variation of normalized in-plane shear stress (σ_6^*) through the thickness of the moderately thick ($a/h = 10$) and thick ($a/h = 4$), anti-symmetric $[0^\circ/90^\circ]$ shell ($R/L = 10$) for material type I is presented in Fig. 12. The in-plane shear stress reaches its maximum value at the center of the shell, while it becomes zero at free surfaces as expected.

Figs. 13 and 14 contain the plots of axial stresses (σ_1^* , σ_2^*) through the thickness, for moderately thick ($a/h = 10$) and thick ($a/h = 4$), symmetric $[0^\circ/90^\circ/90^\circ/0^\circ]$ panel ($R/L = 10$) for material type II. σ_1^* stress reaches its maximum value at the top and bottom surfaces and it is also interesting to state that σ_1^* values are exactly the same for the thick ($a/h = 4$) and moderately thick ($a/h = 10$) panels, but the same is not true for σ_2^* stress. The difference can again be attributed to the in-plane boundary constraints at the edges.

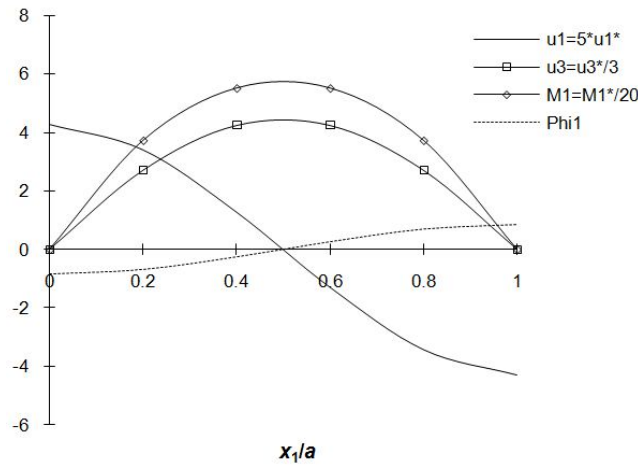


Fig. 11 Variations of displacements, rotation, and moment along the center line, $x_2 = b / 2$, of a moderately thick ($a/h = 10$) antisymmetric $[0^\circ/90^\circ]$ laminate ($R/L = 10$) for material type I

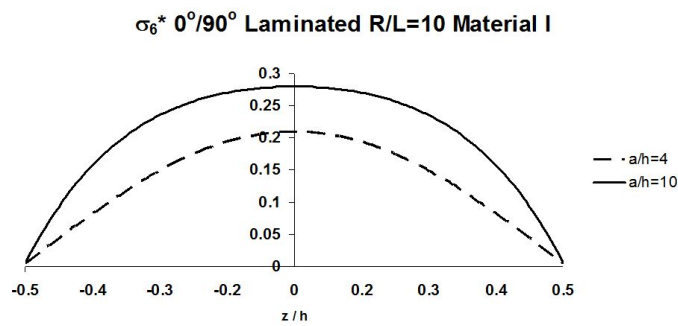


Fig. 12 Variation of normalized in-plane shear stress through the thickness of a moderately thick ($a/h = 10$) and thick ($a/h = 4$), antisymmetric $[0^\circ/90^\circ]$ laminate ($R/L = 10$) for material type I

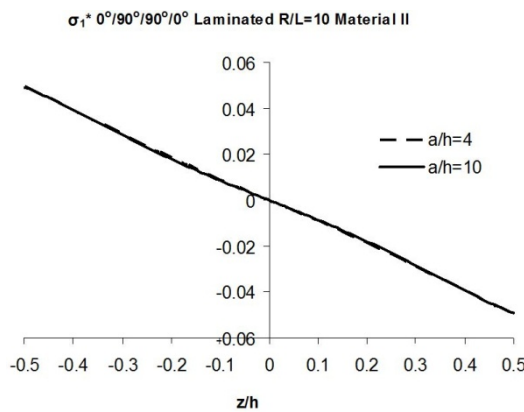


Fig. 13 Variations of normalized stress (σ_1^*) through the thickness of a moderately thick ($a/h = 10$) and thick ($a/h = 4$), antisymmetric $[0^\circ/90^\circ/90^\circ/0^\circ]$ laminate ($R/L = 10$) for material type II

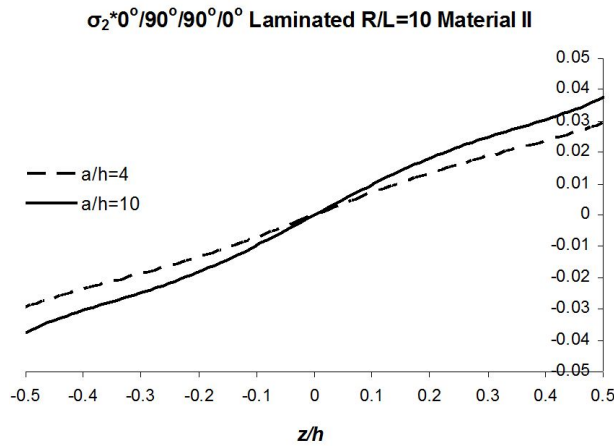


Fig. 14 Variations of normalized stress (σ_2^*) through the thickness of a moderately thick ($a/h = 10$) and thick ($a/h = 4$), antisymmetric $[0^\circ/90^\circ/90^\circ/0^\circ]$ laminate ($R/L = 10$) for material type II

4.2. Sandwich composite material

A finite element model of the sandwich shell is also prepared for a symmetric layup $[0^\circ/90^\circ/\text{core}/90^\circ/0^\circ]$ with core material usage. The comparisons of the present results with finite element counterparts for normalized deflections (u_3^*) with a/h ratio in varying core thickness are presented in Fig. 15 for the material type I at $R/L = 10$. There are negligible differences for the central deflection results between the present theory and the finite element counterparts.

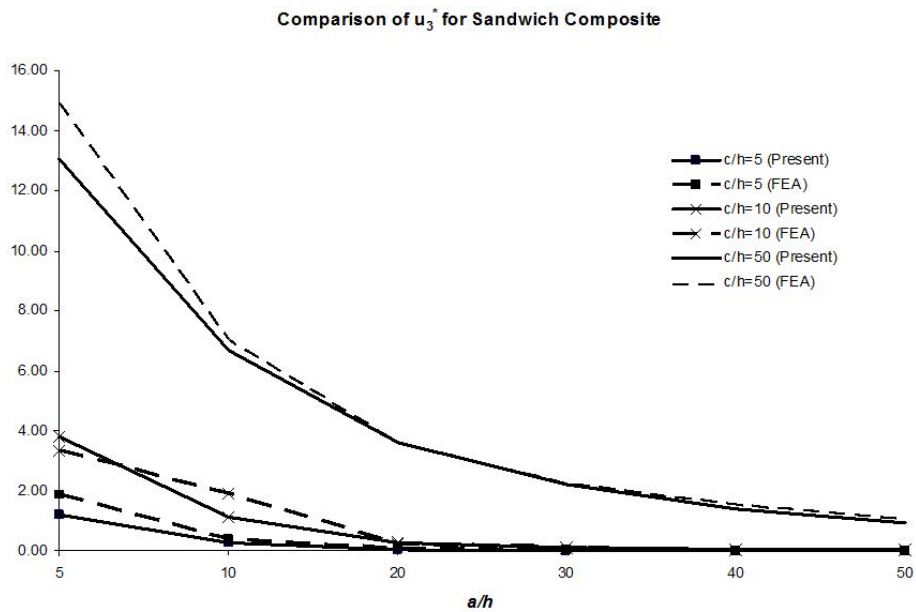


Fig. 15 Comparison of normalized deflection (u_3^*) with finite element solution for material type I, under uniformly distributed load for symmetric sandwich laminate $[0^\circ/90^\circ/\text{core}/90^\circ/0^\circ]$

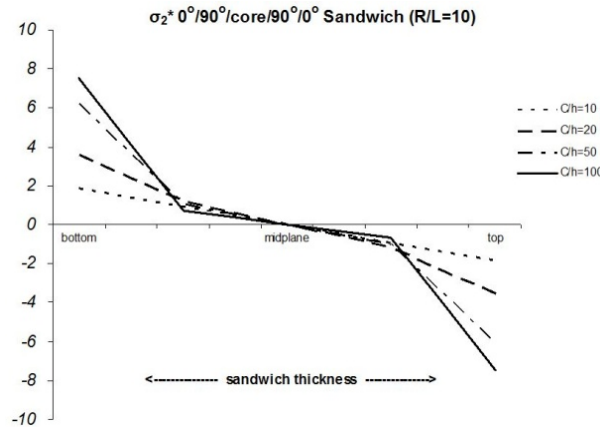


Fig. 16 Variations of normalized stresses (σ_2^*) through the thickness of a moderately thick ($a/h = 10$) symmetric $[0^\circ/90^\circ/\text{core}/90^\circ/0^\circ]$ sandwich laminate ($R/L = 10$) with varying core thicknesses (c/h)

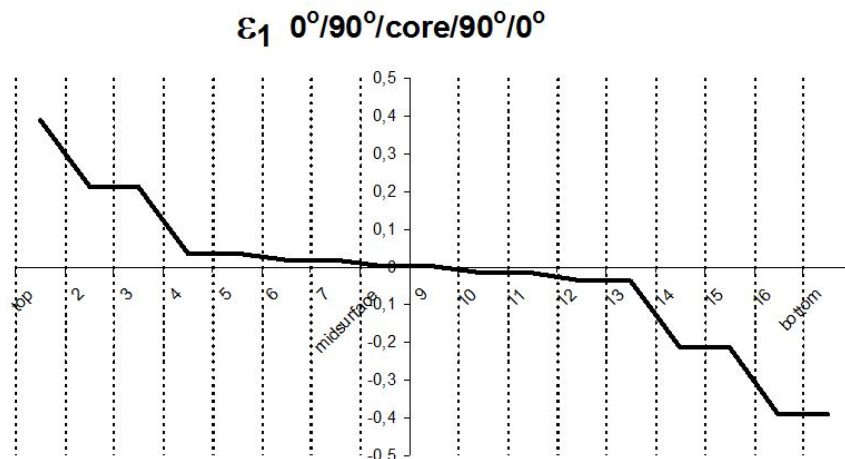


Fig. 17 Variations of strain values (ϵ_1) through the plies of a moderately thick ($a/h = 10$, $c/h = 100$) symmetric $[0^\circ/90^\circ/\text{core}/90^\circ/0^\circ]$ sandwich laminate ($R/L = 10$)

Fig. 16 contains the plots of axial stress (σ_2^*) through the thickness, for moderately thick ($a/h = 10$), symmetric $[0^\circ/90^\circ/\text{core}/90^\circ/0^\circ]$ panel ($R/L = 10$) for material type I with the addition of core material at varying thicknesses. While σ_2^* stress reaches its maximum value at the top and bottom surfaces, the effect of core material thickness is observed at the mid section of the shell.

The changes in the strain values through the laminated plies with the addition of core material for moderately thick ($a/h = 10$), symmetric $[0^\circ/90^\circ/\text{core}/90^\circ/0^\circ]$ shell ($R/L = 10$) for material type I is presented in Fig. 17. The effect of core material with the thickness ratio ($c/h = 100$) can again be observed at the mid section of the shell, while it reaches maximum value at the top and bottom surfaces.

In addition, normalized central deflections and moments of cross-ply symmetric sandwich $[0^\circ/90^\circ/\text{core}/90^\circ/0^\circ]$ shells under uniformly distributed load for sheet material type I at varying

Table 4 Normalized central deflections and moments of cross-ply symmetric sandwich $[0^\circ/90^\circ/\text{core}/90^\circ/0^\circ]$ shells under uniformly distributed load for sheet material type I at varying core thickness

| | R/L | a/h | c/h | | | | | |
|---------|-------|-------|-------|-------|-------|-------|--------|--------|
| | | | 5 | 10 | 20 | 30 | 40 | 50 |
| u_3^* | 10 | 5 | 1.21 | 3.81 | 7.64 | 10.08 | 11.78 | 13.03 |
| | | 10 | 0.27 | 1.12 | 3.12 | 4.67 | 5.82 | 6.69 |
| | | 50 | 0.004 | 0.03 | 0.15 | 0.36 | 0.64 | 0.95 |
| | 50 | 5 | 1.21 | 3.82 | 7.67 | 10.13 | 11.83 | 13.09 |
| | | 10 | 0.27 | 1.13 | 3.16 | 4.73 | 5.89 | 6.77 |
| | | 50 | 0.004 | 0.026 | 0.15 | 0.39 | 0.72 | 1.09 |
| | Plate | 5 | 1.21 | 3.81 | 7.67 | 10.13 | 11.83 | 13.09 |
| | | 10 | 0.27 | 1.13 | 3.16 | 4.73 | 5.89 | 6.77 |
| | | 50 | 0.003 | 0.025 | 0.15 | 0.39 | 0.72 | 1.09 |
| M_1^* | 10 | 5 | 82.68 | 92.72 | 97.31 | 98.67 | 99.15 | 99.31 |
| | | 10 | 56.99 | 77.29 | 91.32 | 96.99 | 99.97 | 101.75 |
| | | 50 | 43.49 | 46.87 | 52.89 | 57.76 | 61.51 | 64.34 |
| | 50 | 5 | 82.84 | 93.04 | 97.73 | 99.12 | 99.59 | 99.75 |
| | | 10 | 57.17 | 77.83 | 92.36 | 98.23 | 101.29 | 103.09 |
| | | 50 | 43.71 | 47.69 | 55.79 | 63.38 | 69.97 | 75.43 |
| | Plate | 5 | 82.84 | 93.06 | 97.75 | 99.14 | 99.61 | 99.77 |
| | | 10 | 57.18 | 77.86 | 92.40 | 98.28 | 101.34 | 103.15 |
| | | 50 | 43.72 | 47.72 | 55.92 | 63.64 | 70.36 | 75.96 |
| M_2^* | 10 | 5 | 41.58 | 39.72 | 37.39 | 36.16 | 35.56 | 35.25 |
| | | 10 | 49.49 | 45.27 | 40.23 | 36.84 | 34.63 | 33.15 |
| | | 50 | 43.09 | 44.84 | 45.68 | 44.49 | 42.48 | 40.32 |
| | 50 | 5 | 41.66 | 39.85 | 37.56 | 36.32 | 35.72 | 35.41 |
| | | 10 | 49.63 | 45.57 | 40.67 | 37.31 | 35.08 | 33.59 |
| | | 50 | 43.28 | 45.53 | 47.95 | 48.47 | 47.89 | 46.81 |
| | Plate | 5 | 41.66 | 39.86 | 37.56 | 36.33 | 35.72 | 35.41 |
| | | 10 | 49.64 | 45.58 | 40.69 | 37.32 | 35.10 | 33.61 |
| | | 50 | 43.29 | 45.56 | 48.05 | 48.64 | 48.14 | 47.13 |

core (c/h) thickness are presented at Table 4 for benchmark purposes. The effect of core layer addition on the normalized central deflection of the shell is remarkable.

5. Conclusions

A new higher-order theory based analytical solution to the boundary problem of an anisotropic composite doubly curved panel is presented. The boundary-discontinuous generalized double Fourier series approach is used to solve highly coupled linear partial differential equations with the mixed simply supported type 1 and type 4 boundary condition prescribed at all four edges. The

results of the analytical solution for cross-ply laminated composite shell under uniformly distributed load are compared with the finite element counterparts and they are in close agreement for both the antisymmetric and symmetric laminations. Additional results under uniformly distributed load and single point load at the center are presented and they are expected to be practically important particularly in the initial design stages of composite structures, and to provide comparisons with numerical results such as finite element, boundary element and meshless methods. Furthermore, numerical analyses for sandwich shells under the effect of identical boundary conditions at varying thickness ratios of the core material under pressure load are presented. The effect of core thickness on the stress values are plotted providing benchmark solutions at pre-design stages.

References

- Carrera, E. (1999), "A study of transverse normal stress effect on vibration of multilayered plates and shells", *J. Sound Vib.*, **225**(5), 803-829.
- Carrera, E. (2000), "An assessment of mixed and classical theories on global and local response of multilayered orthotropic plates", *Compos. Struct.*, **50**(2), 183-198.
- Carrera, E., Cinefra, M. and Nali, P. (2010), "MITC technique extended to variable kinematic multilayered plate elements", *Compos. Struct.*, **92**(8), 1888-1895.
- Catapano, A., Guinta, G., Belouettar, S. and Carrera, E. (2011), "Static analysis of laminated beams via a unified formulation", *Compos. Struct.*, **94**(1), 75-83.
- Chaudhuri, R.A. (2002), "On the roles of complementary and admissible boundary constraints in fourier solutions to boundary-value problems of completely coupled R^{th} order PDE.'s", *J. Sound Vib.*, **251**(2), 261-313.
- Chen, C.S. (2007), "The nonlinear vibration of an initially stressed laminated plate", *Compos.:Part B*, **38**(4), 437-447.
- Cho, M., Kim, K.O. and Kim, M.H. (1996), "Efficient higher order shell theory for laminated composites", *Compos. Struct.*, **34**(2), 197-212.
- Demasi, L. (2012), "Partially zig-zag advanced higher order shear deformation theories based on the generalized unified formulation", *Compos. Struct.*, **94**(2), 363-375.
- Demasi, L. (2013), "Partially layer wise advanced zig zag and HSDT models based on the generalized unified formulation", *Eng. Struct.*, **53**, 63-91.
- Ibrahim, S.M., Carrera, E., Petrolo, M. and Zappino, E. (2012), "Buckling of composite thin walled beams by refined theory", *Compos. Struct.*, **94**(2), 563-570.
- Jones, R.M. (1999), *Mechanics of Composite Materials*, (2nd Ed.), Taylor and Francis, PA, USA.
- Khalili, S.M.R., Davar, A. and Fard, K.M. (2012), "Free vibration analysis of homogeneous isotropic circular cylindrical shells based on a new three-dimensional refined higher order theory", *Int. J. Mech. Sci.*, **56**(1), 1-25.
- Loy, C.T. and Lam, K.Y. (1999), "Vibration of thick cylindrical shells on the basis of three-dimensional theory of elasticity", *J. Sound Vib.*, **226**(4), 719-737.
- Mantari, J.L., Oktem, A.S. and Soares, C.G. (2012a), "A new trigonometric shear deformation theory for isotropic, laminated composite and sandwich plates", *Int. J. Solid. Struct.*, **49**(1), 43-53.
- Mantari, J.L., Oktem, A.S. and Soares, C.G. (2012b), "Bending and free vibration analysis of isotropic and multilayered plates and shells by using a new accurate higher-order shear deformation theory", *Compos.: Part B*, **43**(8), 3348-3360.
- Mantari, J.L., Oktem, A.S. and Soares, C.G. (2012c), "Bending response of functionally graded plates by using a new higher order shear deformation theory", *Compos. Struct.*, **94**(2), 714-723.
- Mantari, J.L., Oktem, A.S. and Soares, C.G. (2012d), "A new trigonometric layerwise shear deformation theory for the finite element analysis of composite and sandwich plates", *Comput. Struct.*, **94**, 43-53.

- Oktem A.S., Alankaya, V. and Soares, C.G. (2013), "Boundary discontinuous fourier analysis of simply supported cross-ply plates", *Appl. Math. Model.*, **37**(3), 1378-1389.
- Reddy, J.N. and Liu, C.F. (1985), "A higher-order shear deformation theory of laminated elastic shells", *Int. J. Eng. Sci.*, **23**(3), 319-330.
- Swanson, S.R. (2001), *Introduction to Design and Analysis with Advanced Composite Materials*, Prentice Hall Inc.
- Tornabene, F., Fantuzzi, N., Viola, E. and Carrera, E. (2014), "Static analysis of doubly-curved anisotropic shells and panels using CUF approach, differential geometry and differential quadrature method", *Compos. Struct.*, **107**, 675-697.
- Tornabene, F., Fantuzzi, N., Bacciocchi M. and Viola, E. (2015), "A new approach for treating concentrated loads in doubly-curved composite deep shells with variable radii of curvature", *Compos. Struct.*, **131**, 433-452.
- Viola, E., Tornabene, F. and Fantuzzi, N. (2013a), "Static analysis of completely doubly-curved laminated shells and panels using general higher-order shear deformation theories", *Compos. Struct.*, **101**, 59-93.
- Viola, E., Tornabene, F. and Fantuzzi, N. (2013b), "General higher-order shear deformation theories for the free vibration analysis of completely doubly-curved laminated shells and panels", *Compos. Struct.*, **95**, 639-666.
- Youssif, Y.G. (2009), "Non-linear design and control optimization of composite laminated doubly curved shell", *Compos. Struct.*, **88**(3), 468-480.
- Zenkour, A.M. (2013), "A simple four-unknown refined theory for bending analysis of functionally graded plates", *Appl. Math. Model.*, **37**(20-21), 9041-9051.

Appendix A. Elements of $[K_{ij}]$ in Eq. (7a)

$$K_{11} = A_{11} \frac{\partial^2}{\partial x^2} + A_{66} \frac{\partial^2}{\partial y^2} \tag{A.1}$$

$$K_{12} = (A_{12} + A_{66}) \frac{\partial^2}{\partial x \partial y} \tag{A.2}$$

$$K_{13} = \left(\frac{A_{11}}{R_1} + \frac{A_{12}}{R_2} \right) \frac{\partial}{\partial x} - c_1 E_{11} \frac{\partial^3}{\partial x^3} - (2c_1 E_{66} + c_1 E_{12}) \frac{\partial^3}{\partial x \partial y^2} \tag{A.3}$$

$$K_{14} = (B_{11} - c_1 E_{11}) \frac{\partial^2}{\partial x^2} + (B_{66} - c_1 E_{66}) \frac{\partial^2}{\partial y^2} \tag{A.4}$$

$$K_{15} = (B_{12} - c_1 E_{12} + B_{66} - c_1 E_{66}) \frac{\partial^2}{\partial x \partial y} \tag{A.5}$$

$$K_{22} = A_{66} \frac{\partial^2}{\partial x^2} + A_{22} \frac{\partial^2}{\partial y^2} \tag{A.6}$$

$$K_{23} = \left(\frac{A_{12}}{R_1} + \frac{A_{22}}{R_2} \right) \frac{\partial}{\partial y} - c_1 E_{22} \frac{\partial^3}{\partial y^3} - (2c_1 E_{66} + c_1 E_{12}) \frac{\partial^3}{\partial x^2 \partial y} \tag{A.7}$$

$$K_{24} = (B_{12} - c_1 E_{12} + B_{66} - c_1 E_{66}) \frac{\partial^2}{\partial x \partial y} \tag{A.8}$$

$$K_{25} = (B_{66} - c_1 E_{66}) \frac{\partial^2}{\partial x^2} + (B_{22} - c_1 E_{22}) \frac{\partial^2}{\partial y^2} \tag{A.9}$$

$$\begin{aligned} K_{33} = & \left[A_{55} - 6c_1 D_{55} + 9c_1^2 F_{55} + c_1 \left(\frac{E_{12}}{R_1} + \frac{E_{22}}{R_2} \right) + c_1 \left(\frac{E_{11}}{R_1} + \frac{E_{12}}{R_2} \right) \right] \frac{\partial^2}{\partial x^2} \\ & + \left[A_{44} - 6c_1 D_{44} + 9c_1^2 F_{44} + 2c_1 \left(\frac{E_{12}}{R_1} + \frac{E_{22}}{R_2} \right) \right] \frac{\partial^2}{\partial y^2} \\ & - 9c_1^2 H_{11} \frac{\partial^4}{\partial x^4} - 2c_1^2 (H_{12} + 2H_{66}) \frac{\partial^4}{\partial x^2 \partial y^2} \\ & - c_1^2 H_{22} \frac{\partial^4}{\partial y^4} - \left[\left(\frac{A_{11}}{R_1^2} + \frac{A_{12}}{R_1 R_2} \right) + \left(\frac{A_{12}}{R_1 R_2} + \frac{A_{22}}{R_2^2} \right) \right] \end{aligned} \tag{A.10}$$

$$\begin{aligned}
K_{34} = & \left[A_{55} - 6c_1 D_{55} + 9c_1^2 F_{55} - \frac{1}{R_1} (B_{11} - c_1 E_{11}) - \frac{1}{R_2} (B_{12} - c_1 E_{12}) \right] \frac{\partial}{\partial x} \\
& + c_1 (F_{11} - c_1 H_{11}) \frac{\partial^3}{\partial x^3} + [c_1 (F_{12} - c_1 H_{12}) + 2c_1 (F_{66} - c_1 H_{66})] \frac{\partial^3}{\partial x \partial y^2} \\
K_{35} = & \left[A_{44} - 6c_1 D_{44} + 9c_1^2 F_{44} - \frac{1}{R_1} (B_{12} - c_1 E_{12}) - \frac{1}{R_2} (B_{22} - c_1 E_{22}) \right] \frac{\partial}{\partial y} \\
& + c_1 (F_{22} - c_1 H_{22}) \frac{\partial^3}{\partial y^3} + [c_1 (F_{12} - c_1 H_{12}) + 2c_1 (F_{66} - c_1 H_{66})] \frac{\partial^3}{\partial x^2 \partial y}
\end{aligned} \tag{A.12}$$

$$\begin{aligned}
K_{44} = & [D_{11} - 2c_1 F_{11} + c_1^2 H_{11}] \frac{\partial^2}{\partial x^2} + [D_{66} - 2c_1 F_{66} + c_1^2 H_{66}] \frac{\partial^2}{\partial y^2} \\
& - (A_{55} + 6c_1 D_{55} + 9c_1^2 F_{55})
\end{aligned} \tag{A.13}$$

$$K_{45} = [D_{12} - c_1 F_{12} + D_{66} - c_1 F_{66} - c_1 (F_{12} - c_1 H_{12}) - c_1 (F_{66} - c_1 H_{66})] \frac{\partial^2}{\partial x \partial y} \tag{A.14}$$

$$\begin{aligned}
K_{55} = & [D_{66} - 2c_1 F_{66} + c_1^2 H_{66}] \frac{\partial^2}{\partial x^2} + [D_{22} - 2c_1 F_{22} + c_1^2 H_{22}] \frac{\partial^2}{\partial y^2} \\
& - A_{44} + 3c_1 D_{44} + 3c_1 (D_{44} - 3c_1 F_{44})
\end{aligned} \tag{A.15}$$